Applied Surface Science 415 (2017) 149–154

Contents lists available at ScienceDirect

Applied Surface Science

journal homepage: www.elsevier.com/locate/apsusc

Full Length Article

Maximum spreading of liquid drop on various substrates with different wettabilities

Raihan Choudhury[a], Junho Choi[a], Sangsun Yang[b], Yong-Jin Kim[b,*], Donggeun Lee[a,*]

[a] School of Mechanical Engineering, Pusan National University, Busan 46241, Republic of Korea
[b] Powder and Ceramics Division, Korea Institute of Materials Science, Changwon 642-831, Republic of Korea

ARTICLE INFO

Article history:
Received 21 August 2016
Received in revised form
21 December 2016
Accepted 24 December 2016
Available online 28 December 2016

Keywords:
Liquid drop impact
Substrate
Wettability
Roughness
Spreading factor

ABSTRACT

This paper describes a novel model developed for a priori prediction of the maximal spread of a liquid drop on a surface. As a first step, a series of experiments were conducted under precise control of the initial drop diameter, its falling height, roughness, and wettability of dry surfaces. The transient liquid spreading was recorded by a high-speed camera to obtain its maximum spreading under various conditions. Eight preexisting models were tested for accurate prediction of the maximum spread; however, most of the model predictions were not satisfactory except one, in comparison with our experimental data. A comparative scaling analysis of the literature models was conducted to elucidate the condition-dependent prediction characteristics of the models. The conditioned bias in the predictions was mainly attributed to the inappropriate formulations of viscous dissipation or interfacial energy of liquid on the surface. Hence, a novel model based on energy balance during liquid impact was developed to overcome the limitations of the previous models. As a result, the present model was quite successful in predicting the liquid spread in all the conditions.

© 2016 Elsevier B.V. All rights reserved.

1. Introduction

The impact of a liquid drop, which we observe in our daily life, plays a major role in many industrial applications such as spray coating, thermal spraying, inkjet printing, and spray cooling [1–3]. Another example is the drop splash during rainfall, which might aid in the propagation of pathogens [4]. During impact, if a drop is massive or its speed of impact is high, the liquid drop splashes into fine droplets. The drop splash, in the sense of droplet generation, looks similar to centrifugal atomization of liquid metal on a rotating disk [5], which is being widely used for industrial-scale production of sub 10-μm metallic powder and even nanoparticles [6–9].

When a spherical drop hits a surface, it rapidly spreads in a circular fashion to form a liquid layer on it. The liquid spreading, though initially driven by the inertia of the falling drop, is continually decelerated by surface tension and viscous forces [10,11], and eventually stops. Subsequently, it can either retract on or remain pinned to the surface, depending on the hydrophobicity of the surface. Of particular interest is the control or maximization of the liquid spreading without splashing. In centrifugal atomization, for example, maintaining the contact between liquid and surface is necessary for maximum utilization of the rotating energy of the surface. In addition, the maximum spreading diameter (denoted hereafter by d_{max}) is directly related to the final coverage and contact time of the liquid with the surface, which in turn influences surface cooling by the liquid [12]. Thus, precise prediction and control of the maximum spreading are critical in applications such as inkjet printing, spray cooling, and centrifugal atomization.

Starting from the Jones' model [13] in 1971, several simple models have been developed to predict a maximum spreading ratio β_{max} ($=d_{max}/d$), based on the energy balance of the drop before and after impact; here d represents the pristine drop diameter. Among those, we chose eight distinct models [13–20] that are distinguished in the formulation of various energy terms involved, as listed in Table 1. Some of the models [17,19,20] enabled fairly accurate predictions with great ease. However, it is noted that: 1) two of them rely on a correction factor [19] or a semi-empirical fitting [20]; 2) previous model validations were mostly conducted in a manner that compares the model predictions with experimental data, without discrimination of the experimental conditions used [17–20]. Thus, it is still necessary to evaluate the models under each specific condition and thereby clarify the conditioned limitation of each model.

Computational fluid dynamics (CFD) simulations have been conducted to predict the transient evolution of the diameter and shape of the liquid layer during the entire process, including the reced-

* Corresponding authors.
E-mail addresses: yjkim@kims.re.kr (Y.-J. Kim), donglee@pusan.ac.kr (D. Lee).

http://dx.doi.org/10.1016/j.apsusc.2016.12.195
0169-4332/© 2016 Elsevier B.V. All rights reserved.

Table 1
Simple models chosen from the previous studies.

Previous models	Formula
Jones	$\beta_{max} = \left(\frac{4}{3}\mathrm{Re}^{\frac{1}{4}}\right)^{\frac{1}{2}}$
Collings et al.	$\beta_{max} = \left(\frac{\mathrm{We}}{6}\right)^{\frac{1}{2}}$
Chandra & Avedisian	$\frac{(9/2)\beta_{max}^4}{\mathrm{Re}} + \frac{3\left[\left(1\text{-}\cos\theta_{static}\right)\beta_{max}^2\text{-}4\right]}{\mathrm{We}} = 1$
Madejski	$\frac{3\beta_{max}^2}{\mathrm{We}} + \frac{1}{\mathrm{Re}}\left(\frac{\beta_{max}}{1.2941}\right)^5 = 1$
Pasandideh-Fard et al.	$\beta_{max} = \sqrt{\frac{\mathrm{We}+12}{3\left(1\text{-}\cos\theta\right)+4\left(\mathrm{We}/\sqrt{\mathrm{Re}}\right)}}$
Kurabayashi–Yang	$\frac{\mathrm{We}}{2} = \frac{3}{2}\beta_{max}\left[1+\frac{3\mathrm{We}}{\mathrm{Re}}\left(\beta_{max}^2\ln\beta_{max}\text{-}\frac{\beta_{max}^2\text{-}1}{2}\right)\left(\frac{\mu_{drop}}{\mu_{wall}}\right)^{0.14}\right]\text{-}6$
Healy et al.	$\beta_{max} = \beta_{max,KY} \times \left(\frac{45^\circ}{\theta_{static}}\right)^{0.241}$
Mao et al.	$\left[\frac{1}{4}\left(1\text{-}\cos\theta_{static}\right)+0.2\frac{\mathrm{We}^{0.83}}{\mathrm{Re}^{0.33}}\right]\beta_{max}^3\text{-}\left(\frac{\mathrm{We}}{12}+1\right)\beta_{max}+\frac{2}{3} = 0$

ing stage [12,17,21]. Those CFD simulations are clearly helpful in understanding the underlying mechanisms of liquid spreading, by providing velocity and pressure fields in the liquid layer. However, it is also noted that CFD simulations, besides its large calculation load, require an accurate prediction of the dynamic contact angle [12,17]. With a static contact angle, the CFD simulations were found to overpredict the maximum spreading significantly, unlike the simple models [19]. Hence, an improved simple model is required not only for industrial applications, but also for more complicated simulations like centrifugal atomization.

These needs motivated the present study. A series of experiments was conducted under precise control of the entire parameters, including roughness and wettability of the dry surfaces. The eight existing models were then tested to assess their validity and limitations depending on the experimental conditions. In comparison with the experimental data, only one model [13] showed a relatively good match for the entire set of conditions, whereas the others had limited success with conditional preferences. A comparative scaling analysis was conducted to elucidate the condition-dependent prediction characteristics of the models. Based on the results, a novel model was finally developed to overcome the limitations of the previous models. As a result, the present model was quite successful in predicting β_{max} in the entire set of conditions including various literature data.

2. Experimental setup

A series of experiments was conducted for the measurement of liquid spreading on a surface upon drop impact as follows. Deionized water was used as the impacting liquid. Three different types of flat surfaces were selected to alter the surfaces' wettability: parafilm wax (Daihan, No: N05042000009323), PMMA (Daihan, No: N05042000007278), and a glass slide (Daihan, No: N05042000007977). The surface contamination could influence the contact angle and model predictions; therefore, the surfaces were carefully cleaned following four sequential steps: rinsing with DI water, 60-min ultrasonication with 10% methanol-water mixture, rinsing with DI water, and complete drying for 24 h at room temperature. The roughness of the as-cleaned dry surfaces was measured with a contact profilometer (Talysurf Series 2, Taylor Hobson) and then positioned on a horizontal test plate as shown in Fig. 1. Needles of three different sizes were used to control the drop diameter and likewise cleaned. Each needle, after being connected to a DI-water filled syringe and a syringe pump (NE-300, SyringePump), was vertically mounted at a certain height from the surface as shown in Fig. 1. Based on the pendent drop method, a controlled amount of liquid was supplied through the needle by the syringe pump and an individual drop of a certain size was generated and allowed to fall onto the surface.

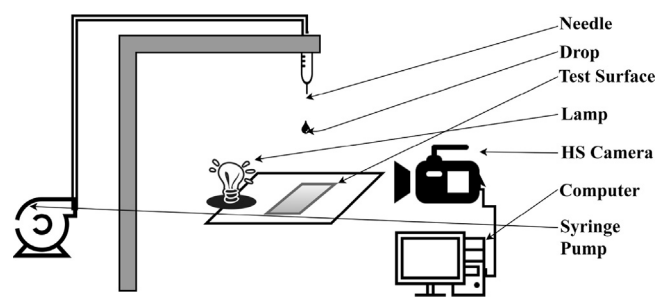

Fig. 1. Schematic for experimental setup.

A contact angle analyzer (SCO model, Phoenix 300) was used to measure the equilibrium contact angle of the water drop; this was repeated three times for drops of three different sizes, leading to an average contact angle for each surface. A Flolight Microbeam 128 LED panel was installed as a light source on one side of the surface-mounted plate. On the opposite side, a high-speed camera (Photon Fastcam, SA3) was installed at 5° from the horizontal surface, and it captured the snapshots at the moment of drop impact with a frame rate of 10,000 fps using the silhouette method. The entire system, schematically shown in Fig. 1, was contained in an acrylic box.

The (drop-falling) height was varied from 10 to 30 cm, to control the impact speed of drop from 1.1 to 2.3 m/s equally for every surface. Based on the snapshots of a falling drop, the diameter (d) of the

Table 2
Experimental conditions and parameters.

Drop-falling height used	10 cm	20 cm	30 cm
Needle size	16 Gauge	25 Gauge	32 Gauge
Mean diameter of drop (d)	3.28 mm	2.70 mm	2.20 mm
Density of water (ρ)	1000 kg/m^3		
Surface tension (γ_{LV})	0.0728 N/m		
Viscosity (μ)	0.00089 Pa s		
Surface material	Parafilm M	PMMA	Glass slide
Contact angle (θ)	104.36°	59.79°	10.12°
Roughness (r_a)	0.82 μm	0.023 μm	0.0089 μm

drop was calculated by an equation of $d = (D_h^2 * D_v)^{1/3}$ [20,22–26], where D_h and D_v refer to the horizontal and vertical diameters of a small ellipsoidal drop as observed at the moment of impact, respectively. The shape was consistent with findings from other literatures [25,27]. The spreading diameter of a drop after the impact was calculated from the snapshots with the help of ImagJ™ and simple Matlab™ code provided by the manufacturer. The liquid properties and the entire systematic parameters are summarized in Table 2.

3. Model formulation

The system energy at any instant of spreading includes the kinetic and surface energies of the spreading liquid. While a drop continues to deform the part of the sphere in touch with the surface to a circular film, the surface energy steadily increases by extending the liquid surface; however, its kinetic energy decreases. Besides, the total system energy is not conserved due to the viscous dissipation of energy. By including the viscous dissipation energy (E_{visc}), the total energy conservation becomes:

$$E_{K,i} + E_{L,i} + E_{S,i} = E_{K,f} + E_{L,f} + E_{S,f} + E_{visc} \tag{1}$$

In Eq. (1), the subscripts i and f refer to the initial state right before impact and the final state at which the liquid eventually reaches the maximum spreading, respectively; E_k refers to the kinetic energy of the drop; E_L is the free surface energy of the liquid (corresponding to its surface tension γ_{LV}); E_S is the interfacial energy between the liquid and the surface.

The three initial energies are generally formulated as follows:

$$E_{K,i} = \frac{\pi}{12}\rho d^3 u^2 \tag{2}$$

$$E_{L,i} = \pi d^2 \gamma_{LV} \tag{3}$$

$$E_{S,i} = \frac{1}{4}\pi d_{\max}^2 \gamma_S \tag{4}$$

$$E_{K,f} = 0, \tag{5}$$

where γ_s is the surface energy density of a dry surface in units of J/m^2. Thus, $E_{S,i}$ is involved in the reflection of the dry part of the surface that will be covered by the liquid in the final state. Eq. (5) implies that the liquid is assumed to stop moving in the final state.

In most of the previous models, the liquid layer in the final state was assumed to be a thin coin-like disk with a flat top surface and sharp edges. Several images taken at that moment revealed that the layer is more likely a spherical cap, i.e. a thin slice of a sphere, with a curved top surface and a flat bottom (see Fig. S1 in the supplementary data). Ford and Furmidge [28] and Vadillo et al. [29] presented an analytic equation to show the spreading ratio β as a function of the contact angle (θ) between the top and bottom surfaces as:

$$\beta = \sqrt{g(\theta)} = \left[\frac{4(\sin\theta^*)^3}{2 - 3\cos\theta^* + (\cos\theta^*)^3}\right]^{1/3} \tag{6}$$

Note that here the contact angle θ was replaced with θ^* to highlight the fact that one may have to use an apparent contact angle θ^* rather than a literature value, particularly when the surface is roughened, and not perfectly smooth (refer to Eq. (12)). Using the spherical cap assumption and Eq. (6), the free surface energy ($E_{L,f}$) is given by:

$$E_{L,f} = \frac{1}{2}\pi\left(\frac{1}{1+\cos\theta^*}\right) g(\theta)\, d^2 \gamma_{LV} \tag{7}$$

The interfacial energy $E_{S,f}$ at the final state is given by the product of the interfacial energy density (γ_{SL}) and the bottom surface area as:

$$E_{S,f} = \frac{1}{4}\pi d_{max}^2 \gamma_{SL} \tag{8}$$

There were several variations in formulating the viscous dissipation energy term E_{visc} in Eq. (1), which are still in debate. Based on the approximation of Chandra and Avedisian [15], Mao et al. [20] proposed the first approximated formula of E_{visc} as

$$E_{visc} = \int_0^{t_c}\int_\Omega \phi d\Omega dt \approx \phi\Omega t_c \approx \left(\frac{\partial u}{\partial y}\right)^2 \Omega t_c \approx 0.53\frac{\pi\mu u d_{\max}^4}{d^2}, \tag{9}$$

where ϕ is the viscous dissipation function, which is proportional to the square of the velocity gradient at the surface; t_c is the time taken for a spherical drop to reach the maximum spread; and Ω is the volume of the viscous layer. Pasandideh-Fard [17] scaled them as $\phi \sim \mu(u/\delta)^2$, $t_c \sim 8/3(d/u)$, and $\Omega \sim \pi d_{max}{}^2\delta/4$, by approximating the flow field during the drop impact with a stagnation-point flow and using the idealized flow solution ($\delta = 2d/Re^{1/2}$); here, the boundary layer thickness δ could grow fast to approach the liquid layer thickness (h) when the Reynolds number ($Re = \rho ud/\mu$) is low or the flow is highly viscous. Hence, Mao et al. [20] proposed two different equations for E_{visc} when Re is small and large; actually Eq. (9) is the case of low Re ($\delta > h$). In contrast, for high Re condition, i.e., $Re > 81(d_{\max}/d)^4$, the E_{visc} is approximated by Eq. (10):

$$E_{visc} = 0.33\frac{\pi\mu u^2 d d_{max}^2}{\sqrt{Re}} \quad \text{if } Re > 81(d_{\max}/d)^4 \tag{10}$$

Since the two energy densities of γ_S and γ_{SL} in Eqs. (4) and (8) are usually unknown, we used Young's equation to relate the difference between them to the measurable values of γ_{LV} and θ:

$$\cos\theta = \frac{\gamma_s - \gamma_{SL}}{\gamma_{LV}} \tag{11}$$

Note that the angle θ in Eq. (11) is the intrinsic contact angle of the liquid on a perfectly smooth surface. For a more realistic surface with a certain degree of roughness, the measurable (apparent) contact angle θ^* usually differs from the Young's contact angle θ due to the surface roughness effect on the hydrophobicity of the surface. This roughness effect on the contact angle was modelled by Wenzel [30] as:

$$\cos\theta^* = \varepsilon cos\theta, \tag{12}$$

where ε is the roughness factor that was approximated in this study by the ratio between the pristine drop diameter (d) and the surface roughness (r_a) as:

$$\varepsilon = \frac{d}{r_a} \tag{13}$$

Since $\varepsilon > 1$, Eq. (12) indicates that a rough hydrophilic surface with $\theta < 90°$ becomes more hydrophilic, while a rough hydrophobic surface with $\theta > 90°$ increases its hydrophobicity.

Now, combining Eqs. (2)–(13) with the energy balance equation, Eq. (1), we obtain the following two sets of equations for calculating the maximum spreading ratio β_{max}: Eq. (14) is for the case of low

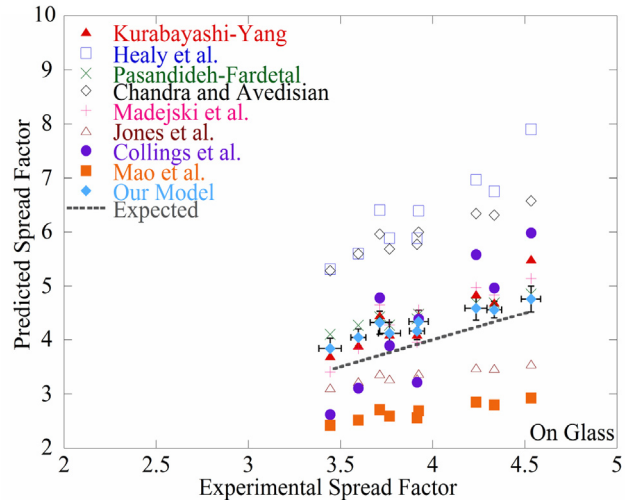

Fig. 2. Validation of the present model and previous models with the present experimental data on glass.

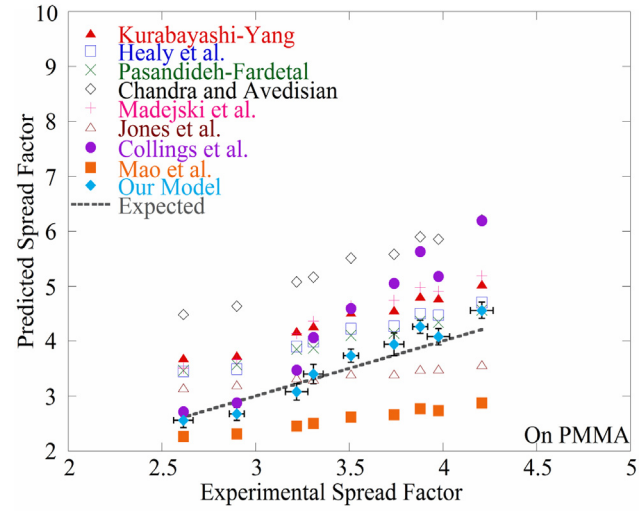

Fig. 3. Validation of the present model and previous models with the present experimental data on PMMA.

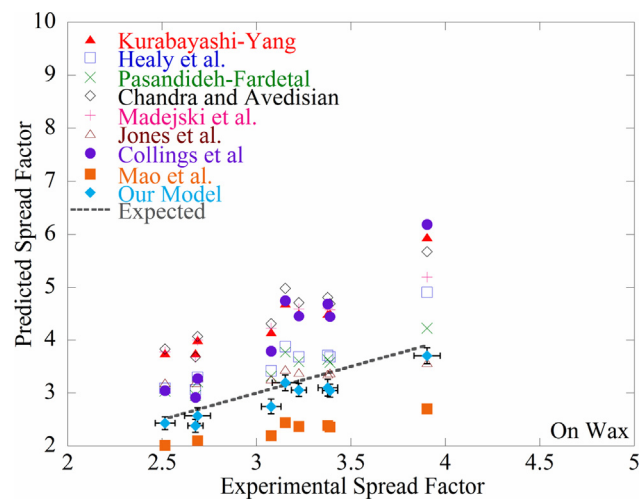

Fig. 4. Validation of the present model and previous models with the present experimental data on wax; the error bars represent standard deviation from experiments and corresponding to their predictions.

Re, while Eq. (15) is for the high *Re* case.

$$0.53\frac{We}{Re}\beta_{\max}^4 + \left(\frac{1}{2}\left(\frac{1}{1+\cos\theta^*}\right) - \frac{1}{4}\frac{\cos\theta^*}{\varepsilon}\right)\beta_{\max}^2 - 1 - \frac{We}{12} = 0 \quad (14)$$

$$\left(0.33\frac{We}{\sqrt{Re}} + \frac{1}{2}\left(\frac{1}{1+\cos\theta^*}\right) - \frac{1}{4}\frac{\cos\theta^*}{\varepsilon}\right)\beta_{\max}^2 - 1 - \frac{We}{12} = 0, \quad (15)$$

where *We* is the Weber number defined by the ratio of the kinetic energy to the free surface energy of liquid drop ($We = \rho u^2 d/\gamma_{LV}$). Both the equations express $\beta_{\max}$ as a function of *Re*, *We*, θ^*, and ε in a similar way as the previous models in Table 1. Eqs. (14)–(15) are obtained by normalizing Eq. (1) with $E_{L,i}$; hence, the first term in both the equations refers to the ratio of $E_{visc}/E_{L,i}$; the second term is the ratio of $E_{L,f}/E_{L,i}$; the third is the ratio of $(E_{s,f} - E_s)/E_{L,i}$; and the fourth term of *We/12* shows the ratio of $E_{k,i}/E_{L,i}$. It should be noted that both the second and third terms include θ^*, so that the second term reflects the combined contributions of the free-surface and interfacial energies, whereas the third term shows the effect of surface roughness.

4. Results and discussion

First, $d_{\max}$ and $\beta_{\max}$ were measured on a dry surface of glass, while the mean diameter and falling speed of a pristine water drop were varied; these experiments were repeated for PMMA and wax surfaces to obtain the data sets of $\beta_{\max}$ under different conditions. Second, the values of *We* and *Re* were calculated for each condition using the determined parameters in Table 2 and then applied to Eqs. (14) or (15) for predicting the β_{max}. To assess the prediction accuracy of the present model, the predicted data of $\beta_{\max}$ on glass, PMMA, and wax were plotted against the corresponding data from experiments using a blue diamond symbol in Fig. 2, Fig. 3, and Fig. 4, respectively. For comparison, the eight existing models in Table 1 were tested with the present parameters for each surface in Table 2. The values of $\beta_{\max}$ predicted by the other models are shown in the figures.

In Figs. 2–4, the vertical axis represents the predicted β_{max}, while the horizontal axis shows the measured β_{max}. The dotted line having a slope of unity indicates a perfect match between the model and experimental values. From Figs. 2–4, one may notice that the largest value of $\beta_{\max}$ decreases with an increase in the surface hydrophobicity. This implies that the water drop can spread more on a hydrophilic surface relative to a hydrophobic surface. It is also noted that the rightmost data in each figure represents the strongest impact condition (the largest drop with the highest impact speed) at each surface; this corresponds to the highest *Re* condition. In contrast, the leftmost data correspond to the lowest *Re* condition.

Mao et al.'s model [20] was found to underpredict the $\beta_{\max}$ constantly, regardless of the surface wettability (as in Figs. 2–4) and operation parameters. Conversely, Healy et al.'s model [19] largely overpredicted the β_{max}, particularly on glass (as in Fig. 2), and the degree of overprediction was lowered on wax (as in Fig. 4). Note that the two models basically rely on either a correction factor [19] or a semi-empirical fitting [20] as shown by the term $(45/\theta)^{0.241}$ *or* $0.2We^{0.83}/Re^{0.33}$ in their formulas given in Table 1. This suggests that these case-specific approaches, though improved the prediction accuracy in their conditions, should be used with great care, because an unexpected conditioned bias could be produced when the condition differs from theirs.

Jones's model [13] exhibited a steady underprediction of $\beta_{\max}$ on glass as seen in Fig. 2; however, it slightly overpredicted under the low-*Re* condition and slightly underpredicted under the high-*Re*

Table 3
Magnitude comparison of various energy components in Eq. (15) at high *Re* number.

Surface	*Re*	*We*	$E_{visc}/E_{L,i}$	$E_{L,f}/E_{L,i}$	$(E_{L,S}\text{-}E_{L,i})/E_{L,i}$	$E_{K,i}/E_{L,i}$
Glass	8053.1	214.9	16.2	5.18	1.26E-05	−18.9
PMMA	8338.9	230.2	14.7	5.89	1.54E-05	−20.2
Wax	8375.1	229.9	12.6	9.25	−1.8 E-04	−20.2

Table 4
Magnitude comparison of various energy components in Eq. (14) at low *Re* number.

Surface	*Re*	*We*	$E_{visc}/E_{L,i}$	$E_{L,f}/E_{L,i}$	$(E_{L,S}\text{-}E_{L,i})/E_{L,i}$	$E_{K,i}/E_{L,i}$
Glass	2795.8	41.2	3.05	2.99	1.16E-05	−4.4
PMMA	3069.9	44.3	1.80	2.27	8.42E-06	−4.6
Wax	3422.5	55.7	1.99	3.84	−1.08E-04	−5.6

condition on the other two surfaces (see Figs. 3 and 4). The predictions of Collings et al.'s model [14] scattered significantly around the ideal line, particularly on glass (as in Fig. 2), and tended to overpredict $\beta_{\max}$ when the surface became more hydrophobic (compare Figs. 2–4). Note that the formulae of their models look simple, being functions solely of *Re* or *We*. To evaluate the appropriateness of their models, it might be helpful to examine the limiting form of a complete energy equation similar to Eqs. (14)–(15). Under a very high *We* condition ($We/Re^{1/2} \gg 1$; often $Re \gg 1$), Eq. (15) is dominated mainly by the first and last terms, leading to $\beta_{max} \sim Re^{1/4}$, which is solely a function of *Re* just like Jones' formula in Table 1. In other words, the Jones' model might be a special solution of Eq. (1) for high *We* condition. It is also noted that the *Re* dependency ($\sim Re^{1/8}$) in Jones's formula is weaker than $\sim Re^{1/4}$ in the limiting case. This seems to explain why Jones's data are almost invariant in each of Figs. 2–4 compared to the other models. Collings et al.'s formula in Table 1 was likewise analyzed. It is noticed that their model is likely another special solution of Eqs. (14) or (15) obtained by neglecting the first term ($E_{visc}/E_{L,i}$). In fact, this is not the case in most experiments, including our experiment.

For a more quantitative discussion, the relative energy terms in Eqs. (14)–(15) were calculated at high and low *Re* conditions, respectively, and summarized in Tables 3 and 4. Table 3 clearly states that the present condition is a high *Re* condition, and the viscous dissipation term E_{visc} dominates every other energy; therefore, that is balanced with the initial kinetic energy $E_{k,i}$. Even in Table 4 where *Re* is small, the term E_{visc} is not negligible but still comparable to the other energy components. This means that all the energy terms should be considered to predict the β_{max}. Thus, it is not surprising to see that Collings et al.'s approach, without considering E_{visc}, caused a significant error. Both tables reveal that the free surface and interfacial energy terms denoted by $E_{L,f}/E_{L,i}$ is large, whereas the contribution of the surface roughness denoted by $(E_{L,S}\text{-}E_{L,i})/E_{L,i}$ is negligible in this study.

Chandra and Avedisian [15], who first introduced the energy dissipation term in the energy balance analysis, approximated the velocity gradient $\partial u/\partial y$ in E_{visc} by u/h under the assumption of creeping flow; u is the falling speed of the drop and h is the liquid layer thickness. According to Pasandideh-Fardetal et al. [17], the choice of h as a length scale for estimating the velocity gradient is not appropriate, because the viscous dissipation occurs mostly in the boundary layer that is developed at the bottom of the liquid layer, and the boundary layer thickness should be used for the length scale instead. They also noted that using h for the estimation of E_{visc} could cause a significant underestimation of E_{visc}, and thereby an overestimation of $\beta_{\max}$ up to 40% [17]. Similarly, Figs. 2–4 confirmed that Chandra and Avedisian [15]'s model reveals a significant level of overestimation of $\beta_{\max}$ in all the conditions considered.

The surface/interfacial energy terms containing θ^* in Eqs. (14)–(15) were missing in the formulas of both Madejski [16] and

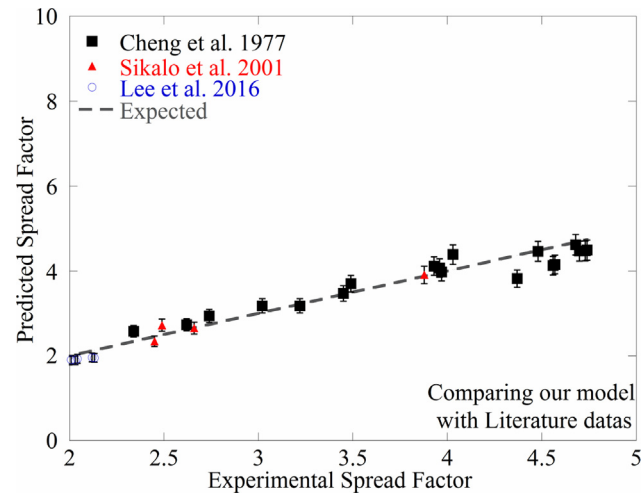

Fig. 5. Comparison of the calculated maximum spread using our model (Eqs. (14)–(15)) with the experimental data in the literature.

Kurabayashi-Yang [19]. Since the missing term $E_{L,f}/E_{L,i}$ increases with an increase in the surface hydrophobicity (see Tables 3 and 4), neglecting this term might cause overprediction of the two models. Consequently, the degree of overprediction becomes worse from Figs. 2–4. According to Bennett et al. [31], model predictions could be improved by including the surface energy in the previous models [14,15]. As stated in Eq. (9), Pasandideh-Fard et al. [17] used the boundary layer thickness as a length scale and a better time scale of $t_c \sim 8/3(d/u)$ for the calculation of E_{visc}. However, their model, similar to Eq. (15) for high-*Re* condition, was still based on the coin-like shape of the liquid layer, which makes the model use in low-Re condition questionable [20]. Figs. 2 and 3 showed that their model prediction errors slightly increased as *Re* decreased (from right to left in the figures), though the errors were still acceptable within 17%.

Figs. 2–4 also demonstrate that the present model is the most successful in predicting the maximum spreading of water, regardless of surface wettability and roughness. Our model was further tested with other literature data under a wider set of conditions: Cheng et al. [32], Sikalo et al. [26], and Lee et al. [12]. Combining their experimental data enables us to test our model in the widest range: in terms of impact velocities (0.2–27.9 m/s), static contact angles (6–105°), surface roughness (0.009–6 μm), and droplet size (0.2–2.7 mm). In Fig. 5, the present model prediction results are denoted by different symbols based on each designated experimental condition and they show a good agreement with all the experimental data within 6%.

5. Conclusion

This study was devoted to the development of a novel energy-balance model for the precise prediction of maximum spreading of liquid at the time of impact on a flat surface. A series of experiments was first conducted to obtain the unknown systematic parameters, by varying the sizes and impact velocities of the water drop, and employing three types of surfaces: glass, PMMA, and wax with controlled surface roughness. Eight previous models were selected and evaluated with the experimental data. Consequently, some of the models were observed to have limited success, with preference to certain conditions. A comparative scaling analysis of the literature models was conducted and it revealed that the four early models [13,14,16,19] suffered from lacks of viscous dissipation and/or surface/interfacial energy, whereas the two recent models [15,17], though included the missing terms, still had a conditional pref-

erence toward high-*Re* conditions by their formations. The other two models [19,20], based on a correction factor or semi-empirical fitting, exhibited relatively large discrepancies, presumably due to the constant use of the case-specific fitting parameters. The present model was developed to resolve the limitations of the previous models. As a result, the present model was quite successful in predicting the liquid spread under the entire set of conditions.

Acknowledgements

This work was supported by the National Research Foundation (NRF) of Korea (No. 2016R1A2B2014141), which is funded by the Ministry of Education, Science and Technology (MEST), Korea, and by the "Development of the Preparation Technology of 0.1 ∼ 10 μm Sized Metal Powders and Fine-Components for Micro Electronics" project of the Korea Research Council for Industrial Science and Technology (ISTK).

Appendix A. Supplementary data

Supplementary data associated with this article can be found, in the online version, at http://dx.doi.org/10.1016/j.apsusc.2016.12.195.

References

[1] F. Froes, C. Suryanarayana, G. Bobeck, E. Lavernia, Innovations in light metals synthesis for the 1990's, in: SAMPE Quarterly, Society of Aerospace Material and Process Engineers, United States, 1991, pp. 22.
[2] E. Gutierrez-Miravete, E. Lavernia, G. Trapaga, J. Szekely, N. Grant, A mathematical model of the spray deposition process, Metall. Trans. A 20 (1989) 71–85.
[3] D. Apelian, Perspectives on process control in powder metallurgy, Met. Powder Rep. 47 (1992) 38.
[4] T. Gilet, L. Bourouiba, Fluid fragmentation shapes rain-induced foliar disease transmission, J. R. Soc. Interface 12 (2015) 20141092.
[5] F.-C. Chou, T.S. Zen, K. Lee, An experimental study of a water droplet impacting on a rotating wafer, Atomization Sprays 19 (2009) 905.
[6] T.A. Saleh, The influence of treatment temperature on the acidity of MWCNT oxidized by HNO 3 or a mixture of HNO 3/H 2 SO 4, Appl. Surf. Sci. 257 (17) (2011) 7746–7751.
[7] M.A. Gondal, T.A. Saleh, Q.A. Drmosh, Synthesis of nickel oxide nanoparticles using pulsed laser ablation in liquids and their optical characterization, Appl. Surf. Sci. 258 (18) (2012) 6982–6986.
[8] S.P. Mates, G.S. Settles, A study of liquid metal atomization using close-coupled nozzles, part 2: atomization behavior, Atomization Sprays 15 (2005).
[9] S.P. Mates, G.S. Settles, A study of liquid metal atomization using close-coupled nozzles, Part 1: gas dynamic behavior, Atomization Sprays 15 (2005).
[10] A. Yarin, Drop impact dynamics: splashing spreading, receding, bouncing, Annu. Rev. Fluid Mech. 38 (2006) 159–192.
[11] M. Rein, Phenomena of liquid drop impact on solid and liquid surfaces, Fluid Dyn. Res. 12 (1993) 61.
[12] J.B. Lee, D. Derome, A. Dolatabadi, J. Carmeliet, Energy budget of liquid drop impact at maximum spreading: numerical simulations and experiments, Langmuir 32 (2016) 1279–1288.
[13] H. Jones, Cooling, freezing and substrate impact of droplets formed by rotary atomization, J. Phys. D: Appl. Phys. 4 (1971) 1657–1660.
[14] E.W. Collings, A.J. Markworth, J.K. McCoy, J.H. Saunders, Splat-quench solidification of freely falling liquid-metal drops by impact on a planar substrate, J. Mater. Sci. 25 (1990) 3677–3682.
[15] S. Chandra, C.T. Avedisian, On the collision of a droplet with a solid surface, Proc. R. Soc. A: Math. Phys. Eng. Sci. 432 (1991) 13–41.
[16] J. Madejski, Solidification of droplets on a cold surface, Int. J. Heat Mass Transfer 19 (1976) 1009–1013.
[17] M. Pasandideh-Fard, Y.M. Qiao, S. Chandra, J. Mostaghimi, Capillary effects during droplet impact on a solid surface, Phys. Fluids 8 (1996) 650.
[18] W.-J. Yang, Theory on vaporization and combustion of liquid drops of pure substances and binary mixtures on heated surfaces, ISAS report 40,15 (1975) 423–455.
[19] W. Healy, J. Hartley, S. Abdel-Khalik, Surface wetting effects on the spreading of liquid droplets impacting a solid surface at low Weber numbers, Int. J. Heat Mass Transfer 44 (2001) 235–240.
[20] T. Mao, D.C.S. Kuhn, H. Tran, Spread and rebound of liquid droplets upon impact on flat surfaces, AIChE J. 43 (1997) 2169–2179.
[21] I.V. Roisman, R. Rioboo, C. Tropea, Normal impact of a liquid drop on a dry surface: model for spreading and receding, Proc. R. Soc. A: Math. Phys. Eng. Sci. 458 (2002) 1411–1430.
[22] J.Y. Li, X.F. Yuan, Q. Han, G. Xi, Impact patterns and temporal evolutions of water drops impinging on a rotating disc, Proc. Inst. Mech. Eng. Part C J. Mech. Eng. Sci. 226 (2011) 956–967.
[23] R. Rioboo, M. Marengo, C. Tropea, Time evolution of liquid drop impact onto solid, dry surfaces, Exp. Fluids 33 (2002) 112–124.
[24] D.C. Roux, J.J. Cooper-White, Dynamics of water spreading on a glass surface, J. Colloid Interface Sci. 277 (2004) 424–436.
[25] S.M. An, S.Y. Lee, Maximum spreading of a shear-thinning liquid drop impacting on dry solid surfaces, Exp. Therm. Fluid Sci. 38 (2012) 140–148.
[26] Š. Šikalo, M. Marengo, C. Tropea, E.N. Ganić, Analysis of impact of droplets on horizontal surfaces, Exp. Therm. Fluid Sci. 25 (2002) 503–510.
[27] Y.-L. Hung, M.-J. Wang, Y.-C. Liao, S.-Y. Lin, Initial wetting velocity of droplet impact and spreading: water on glass and parafilm, Colloids Surf. A: Physicochem. Eng. Asp. 384 (2011) 172–179.
[28] R. Ford, C. Furmidge, Impact and spreading of spray drops on foliar surfaces, Soc. Chem. Ind. Monogr. 25 (1967) 417–432.
[29] D. Vadillo, A. Soucemarianadin, C. Delattre, D. Roux, Dynamic contact angle effects onto the maximum drop impact spreading on solid surfaces, Phys. Fluids (1994-present) 21 (2009) 122002.
[30] R.N. Wenzel, Resistance of solid surfaces to wetting by water, Ind. Eng. Chem. 28 (1936) 988–994.
[31] T. Bennett, D. Poulikakos, Splat-quench solidification—estimating the maximum spreading of a droplet impacting a solid-surface, J. Mater. Sci. 28 (1993) 963–970.
[32] L. Cheng, Dynamic spreading of drops impacting onto a solid surface, Ind. Eng. Chem. Process Design Dev. 16 (1977) 192–197.